# Spectra of magnetic perturbations triggered by pellets in JET plasmas


## FM Poli

E-mail: f.m.poli@warwick.ac.uk
Department of Physics, University of Warwick, Coventry, CV4 7AL, UK.

## PT Lang

Max-Planck-Institut für Plasmaphysik, EURATOM Association, Boltzmannstr. 2, 85748 Garching, Germany

## SE Sharapov, B Alper

EURATOM/UKAEA Fusion Association, Culham Science Centre, Abingdon OX14 3DB, UK

## HR Koslowski

Forschungszentrum Jülich GmbH, Association EURATOM-FZ Jülich, Institut für Plasmaphysik, 52428 Jülich, Germany

## JET-EFDA contributors

See the Appendix of F. Romanelli *et al.*, Fusion Energy 2008 (Proc. 22nd Int. Conf. Geneva, 2008) IAEA, (2008)



**Abstract.** Aiming at investigating ELM pacing for future application on ITER, experiments have been conducted on JET injecting pellets in different plasma configurations, including high confinement regimes with type-I and type-III ELMs, low confinement regimes and ohmically heated plasmas. The magnetic perturbations spectra and the toroidal mode number, $n$, of triggered events are compared with those of spontaneous ELMs using a wavelet analysis to provide good time resolution of short-lived coherent modes. It is found that - in all these configurations - triggered events have a coherent mode structure, indicating that pellets can trigger an MHD event basically in every background plasma. Two components have been found in the magnetic perturbations induced by pellets, with distinct frequencies and toroidal mode numbers. In high-confinement regimes triggered events have similarities with spontaneous ELMs. Both spontaneous and triggered ELMs are seen to start from low toroidal mode numbers, then the maximum measured $n$ increases up to about 10 within 0.3 ms before the ELM burst. The case of MHD events triggered in L-mode and Ohmic phases is also discussed, including similarities and differences with events triggered during H-mode phases.

PACS numbers: 52.25,52.35,52.50,52.55

Submitted to: *Nuclear Fusion*

## 1. Introduction

The high confinement mode (H-mode) plasma configuration [1], reproducible in most tokamaks with a poloidal field divertor configuration, is an envisaged scenario for future operations in ITER. The H-mode is often accompanied by the occurrence of instabilities at the plasma edge, so-called Edge Localized Modes (ELMs), which can be responsible for the loss of particles and energy, and the consequent reduction of the energy confinement time up to 20% [2][3]. Since the energy stored and released by an ELM increases with the tokamak size, it is important for future ITER operations to minimize the damaging effects that ELMs may have on plasma-facing components, by decreasing their amplitude and increasing their repetition rate. One possibility in this direction is the triggering and mitigation of ELMs by pellet injection, already proven successful on the mid-size tokamak ASDEX Upgrade, where, with an appropriate choice of the pellet injection frequency, the repetition rate of ELMs was increased and their amplitude reduced [4]. Aiming at developing a suitable system for ELM pacing with pellets on ITER, experiments with pellet injection were conducted on the larger size tokamak JET with a centrifugal pellet injector [5] and, more recently, with a new high-frequency injector [6], optimized for pellet pacing. These experiments, run in different configurations, including Neutral Beam Injection (NBI) heated H-mode and L-mode plasmas and Ohmic heated regimes, indicate that pellets can trigger coherent MHD activity, which, in H-mode plasmas, can be identified with ELMs. Nevertheless, a few questions still remain open, such as what is the mechanism by which a pellet triggers an ELM, or whether the properties of triggered ELMs depend on the background plasma parameters or they are rather determined by the pellet mass and velocity.
This work addresses the question of how the spectra of magnetic perturbations and the toroidal mode number of pellet-triggered events compare with those of spontaneous ELMs in H-mode plasmas. The analysis of the toroidal mode number spectra is based on wavelets, which provide sufficient time resolution to resolve the evolution of the frequency and toroidal mode number during the short time scales involved. The method, extensively described in [7][8], is briefly reviewed in Sec. 3, where appropriate general bibliographic reference to wavelet analysis is also provided. Wavelet analysis was previously applied on JET to magnetic perturbations and compared with Fourier analysis [9], but never used for mode number analysis of transient events. The experimental setup and the chosen plasma database are introduced in Sec. 2. The spectral features of spontaneous ELMs are compared with those of MHD activity triggered by pellets in H-mode plasmas with compound ELMs (Secs. 4-6), in L-mode and Ohmic plasmas (Sec. 7). Finally, conclusions and future directions are addressed in Sec. 8.

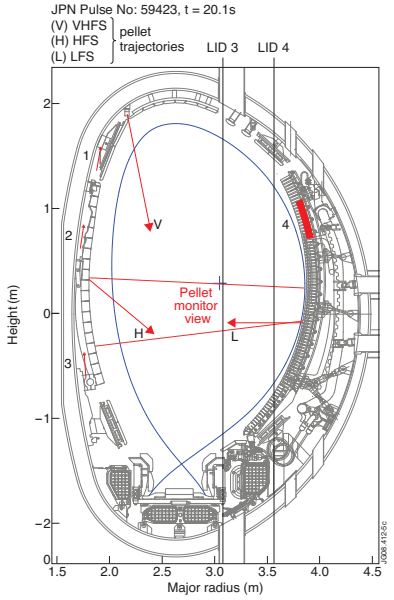


**Figure 1.** (Colour online) Sketch of the poloidal cross-section of JET at octant 2. Also shown is the plasma contour at the last closed flux surface (separatrix) of a typical configuration (JPN 59423) at $t = 20.1$ s, the pellet injection tracks H, V and L, the pellet monitor view, the vertical lines of sight of the interferometer passing close to the plasma core (LID 3) and at the edge (LID 4). Number from 1 to 3 on the inner side indicate the position of inboard pickup coils (at octant 8) while number 4 on the outer side indicates the set of outboard pickup coils (at octant 3).

## 2. Experimental setup

The database analyzed in the following sections includes two examples from the experimental campaign run on JET during 2003 with the centrifugal type pellet injector [5], and two examples from recent experiments run on JET with the new gas gun type High Frequency Pellet Injector (HFPI) [6]. The centrifugal system, operated from 1995 to 2003, was able to inject deuterium pellets with mass of $3.8 \times 10^{21}$ D and speed in the range of 150-300 m/s. The injection trajectories are displayed in Fig. 1 for the three pellet tracks on the JET poloidal cross-section at Octant 2. Pellets are injected through independent guiding tubes from the top (V), from the inboard (H) and from the outboard (L), the guide tube being chosen through a track selector unit at the exit of the pellet centrifuge. Only the vertical and inboard tracks will be considered in this work. The HFPI system is designed for both fuelling and pacing purposes, although experiments have been performed using the fuelling part. Launching at up to 10 Hz repetition rate and at speeds up to $\sim$ 200 m/s was performed from the L and the V tracks. Nominal pellet launch masses range from 2.2 to $3.8\times10^{21}$ D, although only a fraction of $\sim 60\%$ was delivered to the plasma.

Electron density and temperature measurements are provided respectively by a DCN interferometer and by an ECE radiometer, located in Octant 7. The ECE radiation is collected from the low field side, perpendicularly to the magnetic field and along the

major radius, with time resolution of 0.5 ms [10], high enough a value to capture the rapid, large temperature variations associated with pellets and with ELMs. In the rest of the paper, unless otherwise stated, electron temperature is that measured at the top pedestal. The plasma density is integrated along two vertical lines of sight intersecting respectively close to the plasma axis and to the plasma edge, on the low field side, at $R \simeq 3.8$ m. We will refer to these lines of sight as the core density $\bar{n}_c$ and the edge density $\bar{n}_e$.

Poloidal magnetic field perturbations $\dot{B}_p(t)$ are measured on JET by sets of Mirnov coils, mounted on the vessel and close to the plasma surface, distributed along the toroidal and poloidal direction. Two groups of such coils have been used for the measurement of spectra presented herein. The first set includes three high resolution tangential coils, located in Octant 8 and distributed poloidally on the inboard side (numbers 1 to 3 in Fig. 1); the second is located in Octant 3 and includes both toroidally and poloidally distributed coils on the outboard side, at $R = 3.881$ m [11]. The toroidal mode numbers have been extracted from the phase shift of magnetic perturbations measured by two of these outboard edge coils, located respectively at $z_1 = 1.013$ m and $z_2 = 1.005$ m above the midplane, and with orientation $\theta = 108.9$ degrees between the coil axis and the major radius (coils H302 and H303). The coils are separated by $\Delta\varphi = 10.17$ degrees along the toroidal direction, allowing the measurement of toroidal mode numbers up to $|n| = 15$. A pair of pickup coils with smaller toroidal separation of 5.63 degrees is also available, allowing the measurement of higher toroidal mode numbers up to $|n| = 30$ (coils H303 and H304); this pair has a difference of 0.5 degree in the poloidal orientation, so the measured mode number is a combination of the toroidal and of the poloidal component. The effect is negligible during inter-ELM phases and the results from the two pairs of coils coincide in the range of overlapping, for $|n| < 15$. Conversely, during an ELM, when the toroidal mode number can be large, measurements can be affected by the contribution of the poloidal component, $m = nq$. Let $n\phi - m\theta$ indicate the phase of a wave. If, for two probes with coordinates $(\phi_1, \theta_1)$ and $(\phi_2, \theta_2)$, it is $n(\phi_2 - \phi_1) \gg m(\theta_2 - \theta_1)$, the contribution from $\theta$ into the phase of the wave can be neglected. This condition gives an estimate for the ratio $m/n \ll 5.63/0.5 \sim 11$, and for the value of $q$ at which the modes are not affected by $\Delta\theta$. The larger effect is expected for modes localized at the edge, where $q(95\%) = 3 - 4$ in H-mode plasmas, a condition typically encountered on JET.

The $D_\alpha$ emission measured from a telescope on the high field side, indicated in Fig. 1 as pellet monitor, (hereafter $D_{\alpha,P}$) is fairly a good measure of the pellet ablation rate $dN_P/dt$, although only the ablation onset of the inboard pellets is covered by the telescope. The $D_\alpha$ emission measured in the divertor region (hereafter $D_{\alpha,E}$) is instead used as an indication of the occurrence of ELMs.

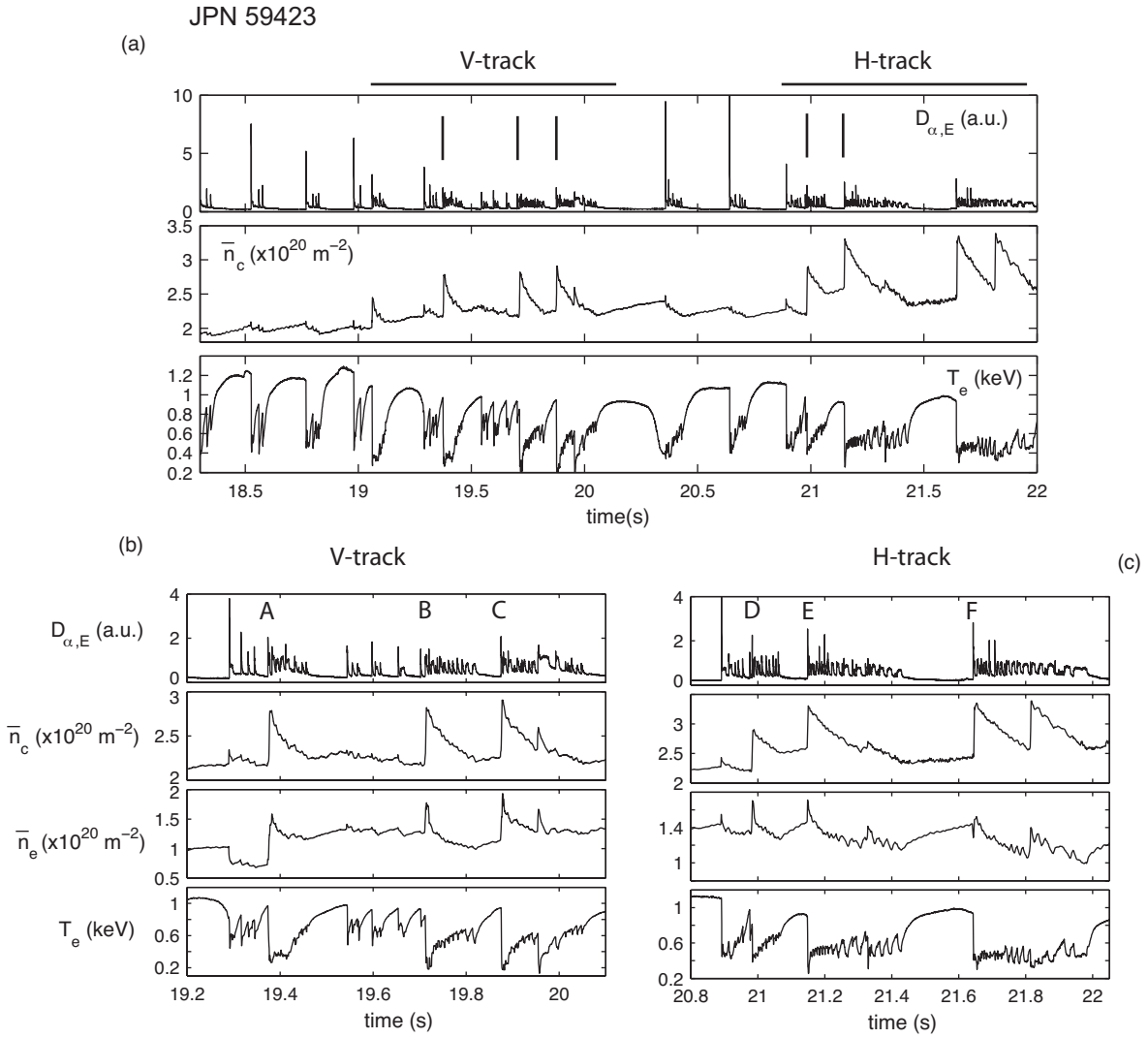


**Figure 2.** JPN 59423: $B_T = 2.4$ T, $I_P = 2.5$ MA, $P_{NBI} = 15$ MW, $P_{RF} = 3$ MW. (a) Time traces of the $D_\alpha$ emission measured in the inner divertor, of the line integrated electron density measured through a line sight intersecting the plasma axis $\bar{n}_{e,c}$ and of the electron temperature $T_e$ measured inside the edge transport barrier, in the pedestal region. Vertical lines in the top plot indicate pellets that are not fragmented. (b) extended view over the time window where pellets are injected from the top (vertical track). (c) extended view over the time window where pellets are injected from the high field side (inboard track). The line integrated density measured at the edge, $\bar{n}_e$, is shown in (b) and (c) for comparison. A-E indicate pellet-triggered events, F indicate a spontaneous ELM almost synchronous with the injection of a pellet.

## 3. Computation of wavelet spectra and extraction of the toroidal mode number

In order to achieve better time resolution in time windows centred on the ELMs, the magnetic perturbation spectra have been computed using a wavelet analysis. Details of the method, as applied to the study of spectral features of ELM precursors on JET

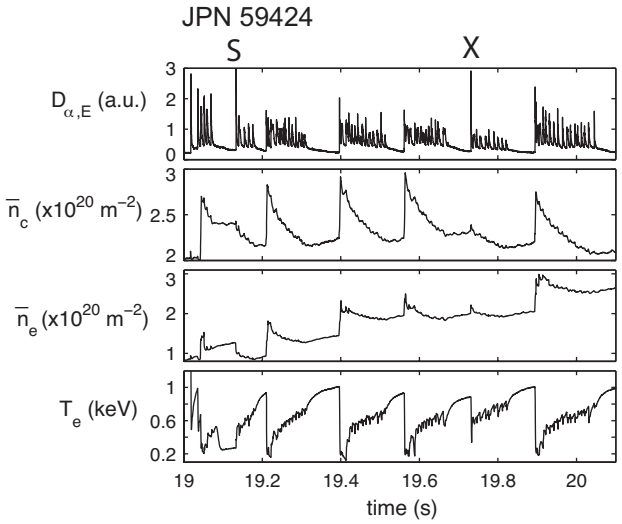


**Figure 3.** JPN 59424: $B_T = 2.4$ T, $I_P = 2.5$ MA, $P_{NB} = 15$ MW, $P_{RF} = 3$ MW. Extended view of the time window where pellets are injected from the vertical track. Time traces of the $D_\alpha$ emission measured in the inner divertor, of the line integrated electron density close to the plasma axis $\bar{n}_{e,c}$, at the edge $\bar{n}_e$ and of the electron temperature $T_e$ measured inside the edge transport barrier, in the pedestal region. 'S' denotes a spontaneous ELM, 'X' a fragmented pellet.

and to the extraction of the toroidal mode number of ELMs are provided in [7][8]. A short summary of the main concepts is given herein for the sake of clarity, referring the reader to the textbook by Mallat [16] for an extensive guide to wavelet analysis and to Ref. [17] for a review of spectral methods applied to the study of MHD and turbulence spectra in plasmas. We have used the Morlet wavelet for the analysis, because of its similarities with Fourier eigenmodes; it is constructed as a sinusoidal wave modulated by a Gaussian function as:

$$\psi(t) = \pi^{-1/4} e^{-t^2/2\sigma^2} e^{\imath\omega_0 t} \tag{1}$$

Values of $\omega_0 = 2\pi$ and $\sigma = 1$ have been chosen to guarantee that the wavelet energy is localized in time, while keeping a large enough number of oscillations under the gaussian envelope. This compromise allows good frequency resolution of short-lived, coherent modes, necessary conditions to study the evolution of spectra during the fast time scales that characterize an ELM. The Morlet wavelet is well suitable for the study of the spectra of transient events, including the evolution of linear and nonlinear spectral features over time scales comparable with the wave period, as discussed in [7].
The continuous wavelet transform (CWT) of a discrete time series $x_k$, of length $N$, sampled at the rate $\delta t$, is defined as the convolution product of $x_k$ with a scaled ($t \to t/s$) and shifted ($t \to t - \tau$) version of $\psi(t)$:

$$W_l(s) = \sum_{k=0}^{N-1} x_k \psi^* \left( \frac{k-l}{s} \delta t \right) \qquad l = 1, \ldots, N-1 \tag{2}$$

Since the Fourier Transform of a convolution product is the product of the Fourier Transforms of the two series, the CWT can be efficiently computed using the Fast Fourier Transform algorithm [16][18]. Scales are chosen as $s = s_0 a^j$, where $s_0 = 2$ is the minimum available scale and, for each value of $j$, $a = 2^{-\nu}$ provides a refining of scales in each *octave* $(2^j, 2^{j+1}]$ [16].

In order to isolate the coherent components of magnetic perturbations and the associated toroidal mode numbers during the ELM crash and during the phases that immediately precede the ELM, we have applied a two-point correlation technique [19], adapted to use wavelet coefficients [20]. After having computed the wavelet coefficients from Eq. (2), the scale-dependent mode number spectrum $P(n, s)$ is reconstructed as follows:

$$P(n,s) = \frac{1}{N}\sum_{l=1}^{N} I[n^l(s) - \bar{n}]P_l(s) \tag{3}$$

where $P_l(s) = 0.5 \times [|W_l(\phi_1, s)|^2 + |W_l(\phi_2, s)|^2]$ is the average of the power spectra measured at time $t_l = l\delta t$ and at positions $\phi_1$ and $\phi_2$, respectively. For each time step $t_l$, the toroidal mode numbers $n^l$ are computed from the phase shift between Mirnov coils divided by their toroidal separation as:

$$n^l(s) = \frac{1}{\Delta\phi}\arg[W_l^*(\phi_1, s)W_l(\phi_2, s)] \tag{4}$$

and compared with the reference values of $\bar{n} = [-15, 15]$. The indicator function $I[n^l - \bar{n}]$, the discrete equivalent of the delta function, is defined as:

$$I[n^l - \bar{n}] = \begin{cases} 1 & \bar{n} \le n^l < \bar{n} + 1 \\ 0 & elsewhere \end{cases} \tag{5}$$

Computing (3) is equivalent to constructing a histogram. The bin width, $\Delta n = 1$, is chosen to minimize the variance in the estimate of (3). Since the value of $n^l(s)$ is weighted by the power spectral density $P_l(s)$, modes with larger amplitude contribute most to the final $P(n, s)$. If, during the time window of length $N\delta t$, the phase shift associated with a spectral component at scale $s$ is coherent, this will results in a large amplitude in the plane $(n, s)$. Conversely, incoherent modes will result in low amplitude $P(n, s)$ values. This method has advantages with respect to standard linear fit over a set of toroidal separated coils in those cases where the mode number structures evolves over short time scales and superposition of modes occur, such as the case of ELMs. The drawback is that this is a local estimate of the toroidal mode number.

## 4. Pellets injected in H-mode plasmas with natural compound ELMs

To start with, let us analyze two examples from the JET experimental campaign run in 2003. In these experiments pellets are injected in type-I ELMy H-mode plasmas, where mostly compound ELMs occur. Although the pellet injection rate was not optimized for pellet pacing, this scenario represents a clear example of the effectiveness of pellets in triggering an ELM. The results obtained herein will therefore be used as a guide for

the interpretation of the spectra measured during more recent experiments, which will be discussed in Sec. 7.

Figures 2-3 show the $D_{\alpha,E}$ emission measured in the divertor region, and the background density and electron temperature in the case of H-mode plasmas JPN 59423 and 59424 in the time window of interest. In both pulses the total heating power is constant and equal to about 18.5 MW, well above the threshold power of about 8 MW for the transition into the H-mode regime. Pellets are injected at the rate of $f_{pel} = 6$ Hz, much lower than the repetition rate of spontaneous ELMs during the pellet-free phase and in similar background plasmas [5]. After a pellet-free phase between 18 s and 19.2 s, pellets are launched from the V-track between 19.2 and 20 s, from the H-track between 20.8 and 22 s, with a short, intermediate pellet-free phase, of approximately 1 s. Pellets that are not fragmented are indicated in Fig. 2(a) with vertical lines. An extended view of the background plasma parameters during the pellet-fuelled phases is shown in Fig. 2(b)-(c) in the case of JPN 59423 and in Fig. 3 in the case of JPN 59424, the latter offering an example of regular train of pellets.

The injection of a pellet is straightforwardly identified by its effects on the background plasma density. The deposition of the ablated material causes a fast increase of the edge and core density, followed by a decrease over longer time scales, comparable to the transport scales. Similarly, the local, imposed cooling causes a fast drop in the electron temperature $T_e$.

Since an ELM causes the degradation of the edge pedestal pressure profile, a drop both in the density and in the temperature occurs over short time scales. Since the density drop associated with an ELM is much lower than the increase that follows the local pellet perturbation, the final, observed effect during a pellet-triggered event is an increase in the edge plasma density. The pellet fuelling impact can therefore be used for monitoring and to separate spontaneous ELMs from triggered events, being the variation of $\bar{n}_e$ negative in the former and positive in the latter case. From the comparison between the core and the edge line integrated density, it can be inferred, for example, that the ELM detected at $t \sim 21.64$ s is not triggered by pellet F (see Fig. 2(c)). Whereas the core density increases, the density measured at the edge increases only after an initial drop. A similar case is also observed in JPN 59424, and in both cases the delay between the occurrence of the ELM and the time where the pellet enters into the plasma is approximately 2.5 ms. This suggests that the presence of an ETB is a necessary condition for triggering an ELM; those pellets that cross the separatrix too shortly after the occurrence of a spontaneous ELM fail to trigger an ELM themselves, because the pedestal is not restored yet.

So-called *compound* ELMs are observed both in the pellet-free and in the pellet-fuelled phase. Compound ELMs are often observed in JET at low densities [12]; they exhibit in the $D_{\alpha,E}$ time trace an initial large spike, followed by a series of smaller spikes. It was suggested that compound ELMs consist of a type-I ELM followed by a series of type-III ELMs [12].

Let us forget - for the time being - this classification and refer only to the position of

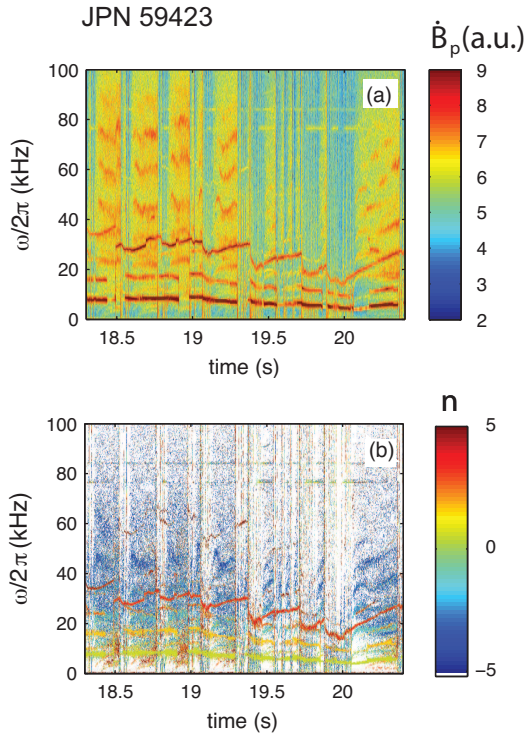


**Figure 4.** (Colour) JPN 59423. (a) Windowed Fourier spectrum, calculated over overlapping time windows of length 2 ms. (b) toroidal mode numbers, extracted from the phase shift between Mirnov pickup coils toroidally separated by 10.17 degrees.

pellet-triggered events in the string of $D_{\alpha,E}$. All pellet-triggered events in JPN 59424 and most of those in JPN 59423 exhibit large $D_{\alpha,E}$ spikes, followed by smaller spikes. These events will be compared with spontaneous ELMs that are the first event in a compound ELM. Exceptions are represented by pellet B injected from the vertical track and pellet D injected from the inboard track (see Fig. 2), which immediately follow the first, spontaneous event in a compound ELMs. The MHD events triggered by these pellets will be compared with the spontaneous events that occupy the same position in a spontaneous compound ELM.

Figure 4 shows the Windowed Fourier spectrum and the toroidal mode number spectrum measured by two outer edge pickup coils, acquired with 1 MHz sampling rate (H302-H303). The Fourier coefficients have been calculated over time windows of 2 ms length, with a 50% overlapping between consecutive windows; the corresponding frequency resolution is about 0.5 kHz. A sawtooth precursor with $n = 1$ is observed at about 8 kHz, and its second harmonic $n = 2$ at higher frequencies. A Neoclassical Tearing Mode (NTM) with $n = 3$ is detected at higher frequencies.

Broadband MHD activity with frequencies up to 100 kHz, propagating along the electron diamagnetic drift direction is observed during the inter-ELM phases. The convention adopted on JET and herein is that positive values of $n$ correspond to modes propagating along the ion diamagnetic drift direction, while negative values of $n$ are associated with modes propagating along the electron diamagnetic drift direction. The level of MHD

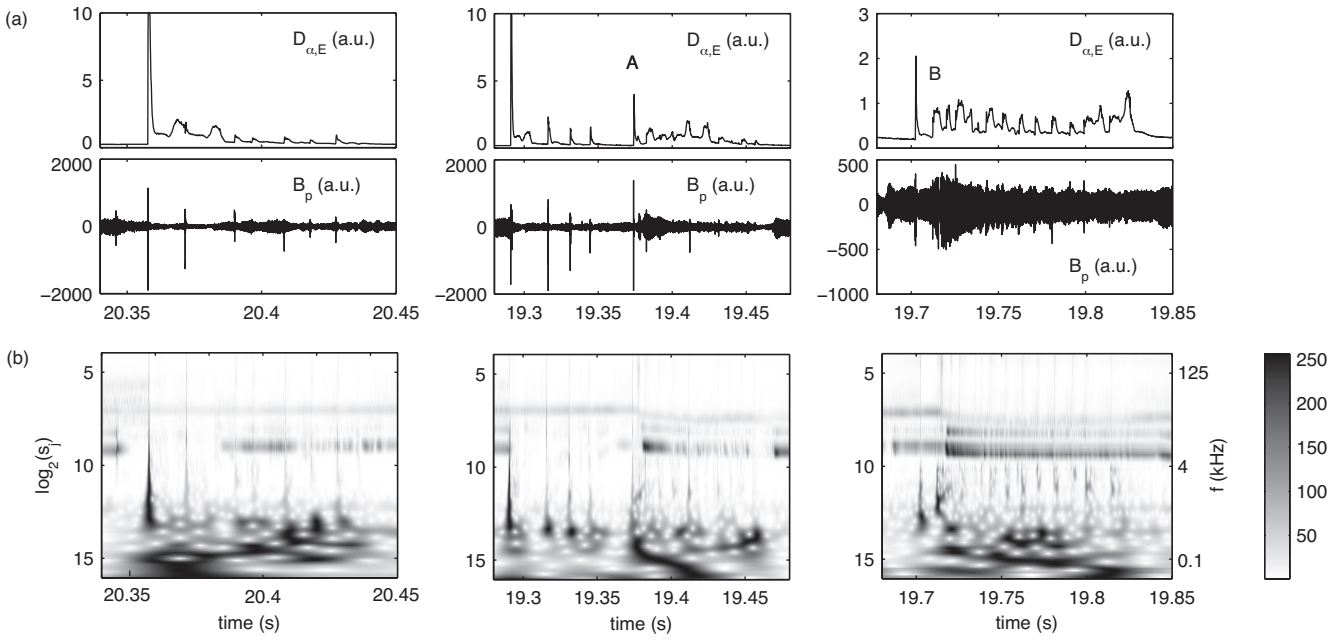


**Figure 5.** JPN 59423. (a) time trace of $D_{\alpha,E}$ measured in the divertor region, and of $\dot{B}_p$ measured on the outboard plane, in the case of spontaneous compound ELMs (left), pellet A (center) and pellet B (right). (b) Wavelet scalogram computed in the same time windows. The sawtooth precursors with $n$=1,2 and the NTM are visible in the wavelet scalogram.

activity with negative toroidal mode number is strongly reduced during the pellet-fuelled phase, although coherent modes with short duration can still be detected during the inter-ELM phases. These modes are likely to be Washboard modes (WB) [14][15]. They are always observed on JET during H-mode plasmas, propagate in the electron drift direction, are localized at the edge and their evolution in frequency follows qualitatively that of the edge electron temperature [14]. In the experiments shown herein, the typical saturation in the WB mode frequency is not observed, most probably because the inter-ELM phase is too short and because the time evolution of temperature is not regular as in the cases studied in Refs. [14][15].

## 5. Spectra of magnetic perturbations of pellet-triggered events

The wavelet spectra of magnetic perturbations of spontaneous ELMs and pellet-triggered events are compared in Fig. 5. The example shows compound ELMs during the pellet-free phase, intermediate between injection from the vertical and inboard track, and two compound ELMs during the time window where pellets are injected from the vertical track (pellets A and B). For graphical representation, the amplitude of wavelet coefficients has been re-normalized to have values bounded in [0,255]; the same scale is used for all the plots, but differences in amplitude between different plots do not reflect real differences in the amplitude of magnetic perturbations. Pellet A enters into the

plasma approximately 30 ms after a spontaneous ELM and it triggers an MHD that is followed by spontaneous, smaller amplitude events. Pellet B enters into the plasma about 10 ms after the first, spontaneous ELM, it triggers an MHD event that is followed by smaller amplitude events. Apart from a different level in the $D_{\alpha,E}$ emission measured in the divertor region, associated with the first event, no differences among the three compound ELMs can be inferred solely from the $D_{\alpha,E}$. The MHD event triggered by pellet B looks to be identical to the first, spontaneous event that follows the event triggered by pellet A, suggesting that the pellet does not modify the structure and the evolution of the compound ELM.

Coherent modes, with frequency below 0.2 kHz, are detected in the wavelet scalogram in all cases, with lifetime much longer than the duration of the ablation phase and, in the case of spontaneous compound ELMs, they are comparable with the duration of the train. These modes, which are most probably not associated with the pellet, are not discussed in this work.

Spontaneous ELMs, such as those that precede pellets A and B, involve modes with frequencies down to 0.2 kHz, with largest amplitude associated with modes in the range of $[0.2, 1]$ kHz. A broadening at large scales is observed in the case of the large amplitude ELM at about 20.35 s, mostly due to the fact that the sampling rate is insufficient to capture the fast growth of this ELM. In fact, as shown in Fig. 6, where the sampling rate is 250 kHz, all the ELMs in the train exhibit the same, apparent broadening, including those with the smallest amplitude.

We can identify at least two differences in the spectra of magnetic perturbations of spontaneous ELMs and pellet-triggered events. First, the magnetic perturbations induced by pellet B in the range of 0.6-2 kHz, have amplitude larger than those associated with spontaneous, small amplitude events in the same train, as shown in the wavelet spectrogram, Fig. 5-(b). The range of frequencies involved and the lowest measured frequencies are instead comparable. Second, a low amplitude, coherent mode is detected after both events A and B. The frequency of the mode, initially $\simeq 1$ kHz ($\log_2(s_j) \simeq 12$), increases with time. There are two possible interpretations to the observed increase in frequency. One is that the plasma has lost its momentum after the ELM crash and that the rotation at the plasma edge is gradually recovering. The second is the impact of the pellet ablation material, which is inert and at rest with respect to the rotating plasma. The lifetime of the coherent mode is about 10 ms in the case of events A and B and it is 20 ms in the case of event C, much longer than the duration of the ablation phase, which is typically below 2 ms. The toroidal mode number of these modes is $n = 1$, and a second harmonic has been observed in the case of the longest lived event. Similar coherent modes are detected also after triggered events in JPN 59424, during injection from the vertical track, but no evidence for them is found in the analyzed shots neither during injection from the inboard track nor after spontaneous, compound ELMs and after isolated, type-I ELMs. Since these modes do not intervene in the triggering of ELMs nor they affect the conclusion of our results, they will not be discussed further.

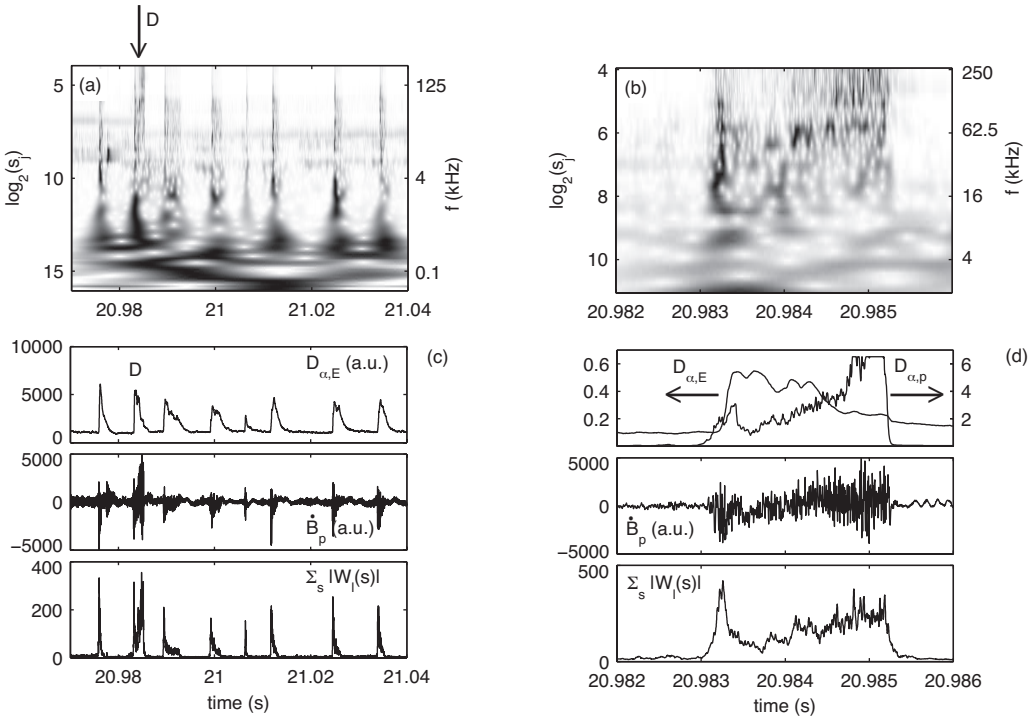


**Figure 6.** JPN 59423. (a) Wavelet coefficients measured during injection from the inboard track. (b) Extended view in a time window centred on the pellet-triggered event D. (c)-(d) time trace of the $D_{\alpha,E}$, $D_{\alpha,P}$, of the absolute value of wavelet coefficients, integrated over frequencies larger than 15 kHz, $\Sigma_s|W_l(s)|$, in the same time window as (a) and (b).

Figure 6 shows the correlation between magnetic perturbations of pellet-triggered events and the measured emission from the ablation cloud. The case of injection from the inboard track is presented here, because measurements from the pellet monitor are available during this time window. Broadband magnetic perturbations are measured during spontaneous ELMs and during the MHD event triggered by pellet D (see Fig. 6(a)). In the latter case, detailed in the expanded view (b), frequencies appear to be lower bounded at about 15 kHz and correlated in time with the duration of the ablation phase, as indicated by a comparison with $D_{\alpha,P}$. The amplitude of magnetic perturbations, integrated over frequencies above 15 kHz, qualitatively follows the time evolution of $D_{\alpha,P}$. It increases over long time scales and decreases over much shorter time scales. This component, as it will be discussed in Sec. 7, is present also in Ohmic and L-mode plasmas and exhibit a similar evolution in time. This suggests that it is independent of the background plasma, but is directly associated with the pellet perturbation; we will refer to it in the rest of the paper as pMHD.

Superposed to the pMHD, a second component is observed, appearing as by a peak between 20.983 and 20.9835 s. As shown in (c), where the integrated spectrum is reported for all the events in the train, the time scales are comparable with those associated with spontaneous ELMs, about 0.3 ms. This component is observed only in H-mode plasmas and has close similarities with spontaneous ELMs that occur in the

same plasma, as it will be discussed more in detail in the next section. This suggests that it is not directly associated with the pellet parameters, although it is a consequence of the presence of the pellet in the plasma; we will refer to it as pELM.
We note that the integrated spectrum shown in Fig. 6 represents only a portion of the spectrum of the magnetic perturbations induced by the pellet, namely those at the highest frequencies. Differences with spectral components at lower frequencies will be discussed in the next section.

## 6. Toroidal mode number spectra of MHD events triggered by pellets

We have analyzed the toroidal mode number spectrum of both the pMHD and the pELM components, for of all pellet triggered events in discharges JPN 59423 and 59424 in the case of injection from the V-track. Since fast acquisition is not available for the outboard coils during the phase of injection from the H-track, the toroidal mode number spectrum has not been analyzed in this case. In all the cases considered herein the toroidal mode number spectra measured during a pELM have been compared with those measured before and after to assess the relative increase of power associated with different components. The scale dependent toroidal mode number spectrum $P(n, s)$ is computed over the time window of interest and normalized to time units for comparison. Integrating over frequencies provides the total toroidal mode number spectrum $P(n)$ associated with spectral component with frequencies in the range of interest.

### *6.1. Toroidal mode number spectrum of pMHD*

Figure 7-(b) shows the toroidal mode number spectrum associated with the pMHD in the case of pellet A (JPN 59423), for spectral components with frequencies between $\simeq$ 15 kHz and 250 kHz ($4 \leq \log_2(s_j) < 8$). Three time windows are considered here: the first (I) is taken right after the pELM, the others (II-III) during the ablation phase, when the level of magnetic perturbations at high frequency becomes significantly larger than the background fluctuation level. During this phase $P(n)$ is peaked at $n = 1, 2$ and asymmetric, with spectral width of approximately $\Delta n = 3$. The value of $n$ at which $P(n)$ is maximum and the power spectral width are comparable for all the pellets injected in JPN 59423 and JPN 59424. Qualitatively similar results have been found on ASDEX Upgrade, where it has been measured that the magnetic perturbations of the pMHD also propagate along the ion drift direction, although the toroidal mode number is $n = 6$ [13]. The spectrum measured right after the pELM is shown for comparison, it is peaked at $n = 3$ and approximately 100 times lower. Although care has been taken to exclude the NTM frequency during the integration of the spectrum, its effect cannot be completely eliminated for at least two reasons. First, the Morlet wavelet produces spectra smoother and wider than Fourier eigenmodes. Secondly, the NTM frequency drops after a pELM, while the lower limit chosen here for the integration of spectra is constant.

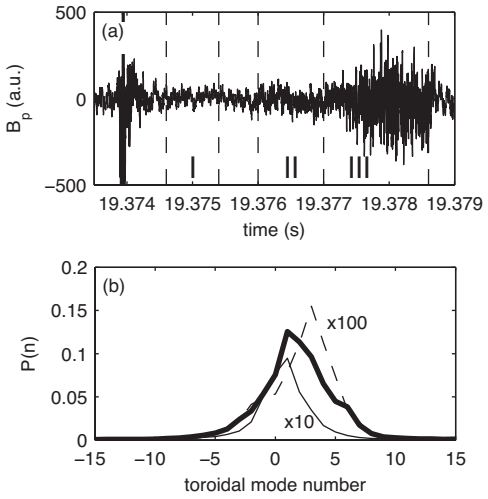


**Figure 7.** JPN 59423. (a) Magnetic perturbations $\dot{B}_p$ measured by the outer edge Mirnov coil H302 in a time window centred on the pellet-triggered event A (see Fig. 2). (b) Toroidal mode number spectrum associated with spectral components at frequencies higher than 15 kHz, computed during time window I (dashed line), time window II (thin line) and during time window III (thick line).

### *6.2. Toroidal mode number spectrum of pELMs*

Figure 8 shows the case of the pELM triggered by pellet C after $f_{pel}^{-1}$ with respect to the previous pELM; no spontaneous type-I ELMs are detected between the two. The $P(n, s)$, shown in (b), is computed over six time windows of approximately 0.1 ms length. No apparent variation in the toroidal mode number value is observed at low frequencies, during the time window of interest; $P(n, s)$ is peaked at $n = 1 - 2$ in the range of scales $\log_2(s_j) \simeq 10 - 14$ (frequencies between 0.25 and 4 kHz), and this value does not change. Conversely, variations in the value of $n$ and in the amplitude of magnetic perturbations are measured at higher frequencies. Initially, only modes with lower values of $|n|$ are detected in the $P(n, s)$. Within 0.3 ms before the crash, progressing from phase I to III, new modes with larger $|n|$ appear, with higher amplitude. According to the convention used, these modes propagate along the electron diamagnetic drift direction. A saturation in the maximum value of $|n|$ occurs immediately before the pELM crash, when the amplitude of magnetic perturbation reaches a maximum, then the mode structure is destroyed during the burst.

The evolution of the toroidal mode number spectrum $P(n)$, obtained from $P(n, s)$ integrating over scales $\log_2(s) = [4, 10]$ (frequencies between 4 and 250 kHz) and in the same time windows, is shown in Fig. 8-(c). For comparison, also shown is the spectrum measured approximately 1 ms before the crash. In this time window, where the dominant contribution to the background MHD activity is represented by the NTM, the spectrum is peaked at low, positive toroidal mode numbers, with a maximum at $n = 3$. The apparent width of the spectrum is mostly due to the gaussian envelope of the Morlet wavelet. A lower amplitude peak is measured in the range of $n = [-7, -3]$,

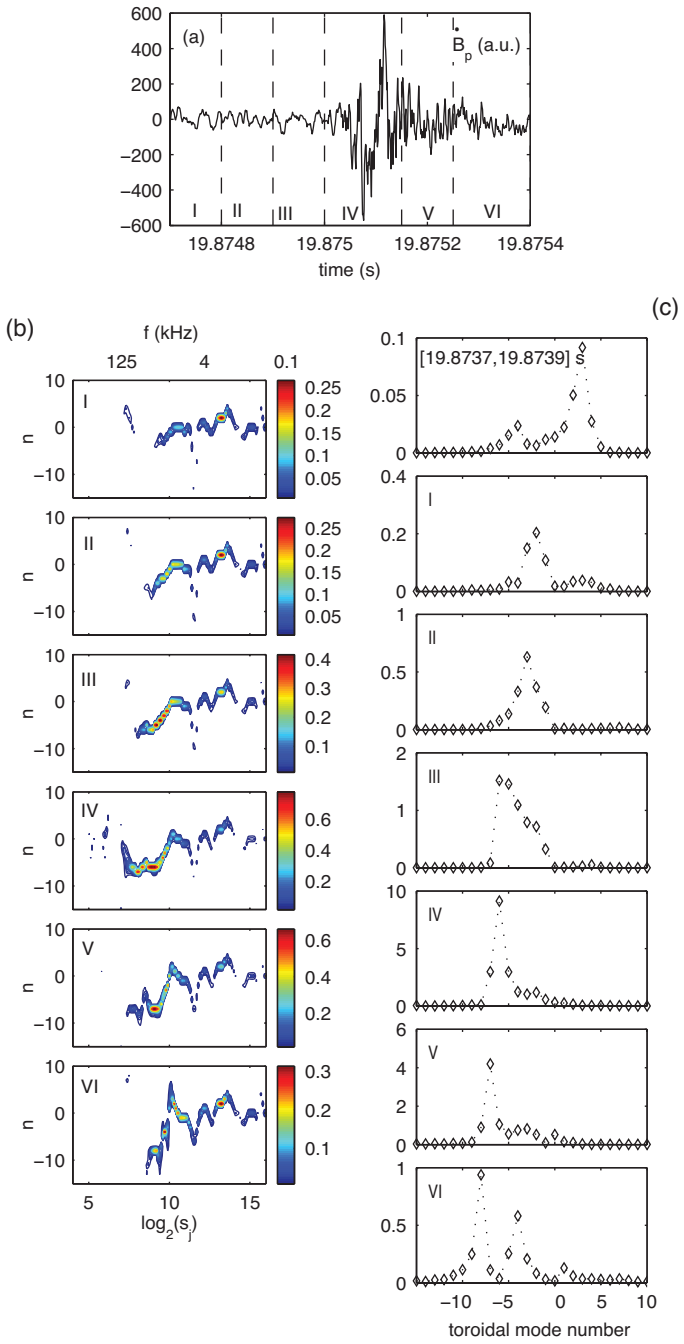


**Figure 8.** (Colour online) JPN 59423, pellet C. (a) time trace of magnetic perturbations $\dot{B}_p$ of the pELM triggered by event C. (c) Scale dependent toroidal mode number spectrum $P(n, s)$, computed over the time windows I-VI, as indicated in (a). (c) Toroidal mode number spectrum, $P(n)$, obtained integrating $P(n, s)$ over scales $\log_2(s_j) = [4, 10]$. For comparison it is also shown $P(n)$ computed 1 ms before the pELM crash (top frame).

with maximum at $n = -4$, likely associated to the WB modes that are present during inter-ELM phases. The power spectral density associated with negative toroidal mode numbers gradually increases, reaching a maximum during the crash, then it rapidly

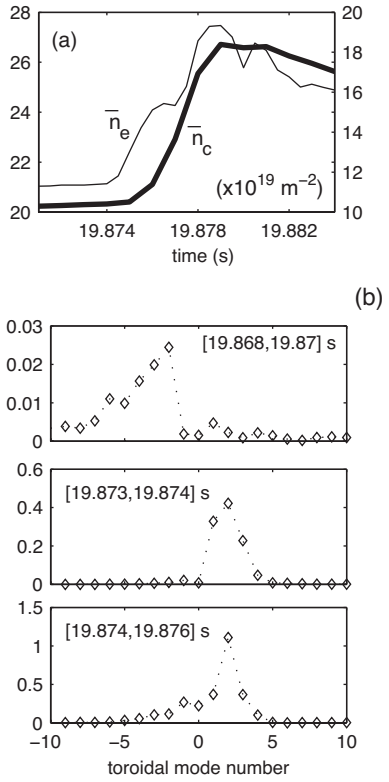


**Figure 9.** JPN 59423, pellet C. (a) time evolution of the core (thick line, left axis) and edge (thin line, right axis) line integrated density (units of $10^{19}$ m$^{-2}$). (f) Toroidal mode number spectrum, $P(n)$, obtained integrating $P(n, s)$ over scales $\log_2(s_j) = [11, 14]$, during the time windows indicated in the plot.

decreases back to values comparable with those measured before the crash. At the same time the value of $n$ at which the spectrum is peaked increases in absolute value up to $|n| = 6$. A similar behaviour has been observed also for the five pellets injected from the vertical track in the time window $[19, 20.2]$ s in JPN 59424. It is observed in these experiments that the power spectrum at negative toroidal mode numbers, in the range of $n = [-10, -1]$ increases immediately before the crash and during the crash, although the value of $n$ at which the power spectrum is peaked may be slightly different for individual events.

It was suggested by Perez *et al* [15] that WB modes may have a regulating effect on the pedestal and a modified peeling-ballooning cycle was proposed to take into account the WB mode phenomenon. It was shown that WB modes may interact with ELM precursors, but it was excluded that can be themselves precursors to the ELMs. The toroidal mode number spectra shown herein do not contradict this picture. For example, should the mode at about $n = -4$ be a precursor, its amplitude would increase while approaching the ELM; this is not observed. It is instead observed that modes with toroidal mode number low in absolute value are the first to appear, then the value of $|n|$ increases, suggesting an independent origin.

Contrary to spectral components with frequency higher than 4 kHz, the toroidal mode

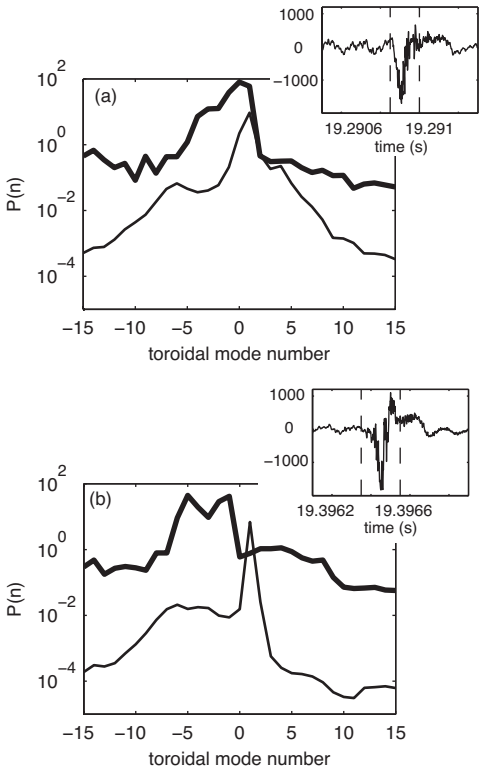


**Figure 10.** Toroidal mode number spectrum of spontaneous (JPN 59423) (a) and triggered ELM (JPN 59424) (b), measured 1 ms before (thin line), and during the ELM (thick line). The insets show the time trace of magnetic perturbations, with vertical dashed lines indicating the time window where the power spectrum is measured.

number spectrum at frequencies below 4 kHz (scales $\log_2(s_j) = [11, 14]$) exhibits a different evolution, as shown in Fig. 9. The chosen range of frequencies excludes contributions from the NTM and from the sawtooth precursors. Compared with the inter-ELM phase, where $P(n)$ is peaked at $n < 0$, in a time window centred on the pELM, $P(n)$ is peaked at $|n| = 1, 2$. The time when $P(n)$ is first observed to peak at $n = 1, 2$ is comparable to the time when the density at the edge starts rising (see Fig. 9).

A note is worth at this point on the timescales of high-frequency and low-frequency perturbations shown here and the error bars in the analysis. The scaling factor used in Eq. (2) allows to adjust the time-frequency resolution in the final scalogram. Although the CWT is computed over each time step, the time resolution is determined by the frequency of the mode. This means, for example, that high frequency modes, associated with shorter time scales, can be better localized in time than low frequency modes. For example, the coherent mode at $\log_2(s) \sim 13$ in Fig. 8(b), has an equivalent frequency of 0.5 kHz, which corresponds to a period of 2 ms. This mode cannot therefore be localized in time with a precision better than its period. This should be taken into account when comparing the time scales of background plasma parameters, such as the line integrated density, with the time windows where spectra of low frequency perturbations

are computed. Comparing Figs. 8-9, it can be inferred that the modes with $n < 0$ - which are first detected during phase I - appear after the low frequency, low $n$ modes shown in Fig. 9, although the exact delay time cannot be estimated with a precision below 1 ms.

Large values of power spectral density at negative toroidal mode numbers have also been measured in the case of the first, spontaneous event of compound ELMs in these plasmas. An example is shown in Fig. 10 in the case of a spontaneous ELM and a pELM. In both cases the spectrum is peaked at $n = 1$ before the ELM crash and the power spectral amplitude associated with components with $n < 0$ is about 100 times higher than that associated with positive toroidal mode numbers. In both cases an increase of the power spectral density associated with negative toroidal mode numbers is measured during a 0.2 ms window for the spectral components with frequencies larger than about 4 kHz. The apparent flattening of the spectrum for large positive and negative toroidal mode number values is mostly due to phase jumps that are measured close to the burst. Contrary to the case when the delay between ELMs is sufficiently long to allow an ETB to develop, when the delay after a spontaneous ELM is short, no clear toroidal mode number is measured for frequencies larger than 4 kHz. The measured magnetic perturbations have low degree of coherency and the toroidal mode number spectrum is peaked at $n = 0$. This is the case for both spontaneous and triggered events that follow the first, large amplitude event in a compound ELM.

To summarize, pellets, when injected with a sufficient delay after a spontaneous ELM, to allow the plasma pressure profile to recover, trigger an MHD event that has spectral features similar to spontaneous ELMs that naturally occur in the same background plasma. A superposition of coherent modes with absolute values $|n| < 10$ is observed, with $|n|$ progressively increasing within the 0.3 ms that precede the crash. The value at which $P(n)$ is peaked also increases approaching the crash, although the peaking value does not necessarily coincide with the maximum measured $|n|$.

## 7. Pellets injected in L-mode plasmas

Figure 11 shows an example of experiment on JET where pellets are injected in L-mode and Ohmic plasmas, the case of JPN 73368 ($B_T = 2.5$ T, $I_P = 2.0$ MA). After an Ohmic phase between 14 and 18 s, the plasma is heated with 6.2 MW of NBI during the time window $[18, 21.5]$ s and with 1.9 MW during $[21.5, 29]$ s. A transition from type-III ELMy H-mode to L-mode confinement occurs at 21.5 s, as a result of the stepping down of the NBI power. Pellets are injected from the low field side, starting from $t \simeq 14.5$ s, approximately every 1 s. Three pellets are injected during the Ohmic phase, two pellets are injected during the H-mode phase, at 19.5 and 20.5 s, one at the H-L transition and two during the L-mode phase, at about 22.5 and 23.5 s, as indicated in the figure. The pellets injected during the Ohmic phase are already fragmented before entering the plasma, while the pellets injected during the L-mode plasma are intact. All these pellets trigger an MHD event, including those fragmented.

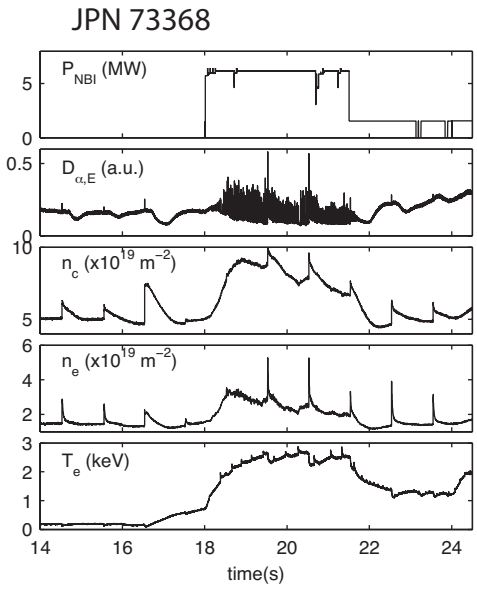


**Figure 11.** JPN 73368. $B_T = 2.5$ T, $I_P = 2.0$ MA, $P_{RF} = 3$ MW. Time traces of the NB injected power (a), of the $D_\alpha$ emission measured in the inner divertor (b), of the line integrated electron density measured at the plasma axis $\bar{n}_c$ (c) and at the edge $\bar{n}_e$ (d), and of the electron temperature $T_e$ measured at 3.4 m.

The spectra of magnetic perturbations induced by the first pellet in L-mode are shown in Fig. 12. A sawtooth precursor at $\sim 4$ kHz and the subsequent crash at $\sim 22.515$ s can be identified before the triggered event, while a coherent mode, with lifetime of 4 ms and frequency of 60 kHz, is detected right after.

Similarly to triggered events in H-mode plasmas, the toroidal mode number spectrum exhibits two distinct components, one in the range of frequencies between 0.12 and 4 kHz, corresponding to scales $\log_2(s_j) = [9, 14]$, the other at higher frequencies. The toroidal mode number spectrum associated with the lower frequency components peaks at $n = 1, 2$, as shown in (c), similarly to what observed in the case of pellets injected in H-mode plasmas. The amplitude of magnetic perturbations, integrated over frequencies larger than 4 kHz, is shown in (d). It is qualitatively similar to the pMHD observed in H-mode plasmas, with rising time longer than decay time. Contrary to H-mode plasmas, the pELM component is not detected in this case. The amplitude of spectral components integrated over low frequencies is shown for comparison; it has constant amplitude during the phase of ablation. The apparent symmetry and the slow rising and decay times of this low-frequency component are mainly associated with the longer period of the associated modes.

Pellets injected during the Ohmic phase are fragmented, with the larger fragments inducing magnetic perturbations over time scales of a few ms. The spectra of magnetic perturbations (not shown here) are similar to those of pMHD events in L-mode plasmas, with a low frequency and a high frequency component, although the degree of coherence is lower and a clear toroidal mode number cannot be identified in this case.

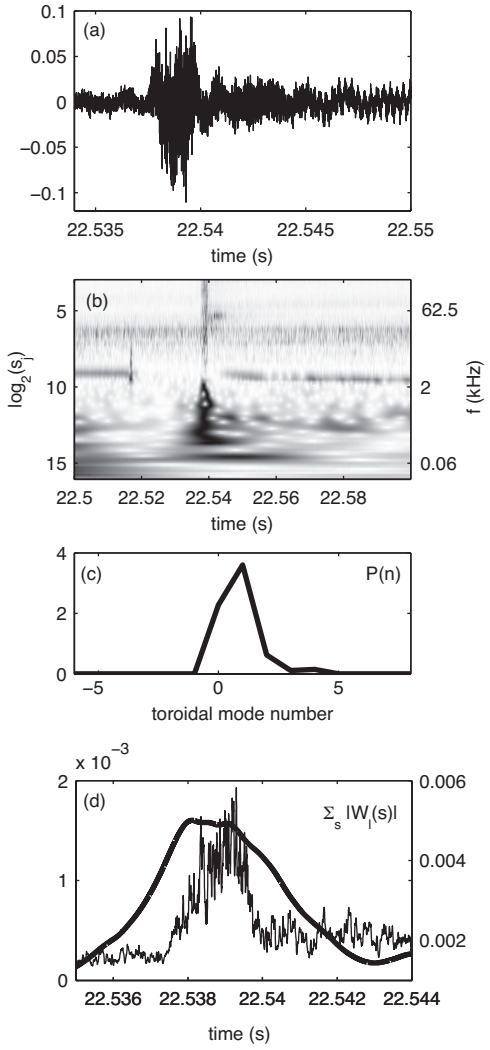


**Figure 12.** JPN 73368, L-mode phase. (a) magnetic perturbations in a time window centred on the triggered event. (b) Power spectral density of magnetic perturbations (arbitrary units) in a window centred on the ELM triggered by pellet C. For graphical purposes data are plotted with the reduced time resolution of 20 $\mu$s. (c) Toroidal mode number spectrum at low frequencies ($\log_2(s_j) = [9.5, 12]$), computed during $t = [22.5385, 22.5395]$. (d) Amplitude of magnetic perturbations (arbitrary units), integrated over frequencies higher than 4 kHz (thin line, left axis) and over frequencies below 4 kHz (thick line, right axis).

## 8. Conclusions

Pellet-triggered MHD is a complex phenomenon, involving at least two time scales in H-mode plasmas. MHD perturbations associated with the pellet ablation effects occur over time scales of a few ms. This component, which we call pMHD, is present in all plasma backgrounds, including Ohmic, L-mode and H-mode plasmas. The magnetic perturbation spectrum of the pMHD can be ideally separated into two parts, one at lower frequencies, the other at higher frequencies, which contains approximately 25% of

the total power spectral energy. Since the pMHD is always present and its is correlated in time with the duration of the pellet ablation phase, we infer that this component is directly associated with the pellet and is only weakly dependent on the background plasma parameters.

A second component is observed only in H-mode plasma: it occurs over shorter time scales, typically 0.2-0.3 ms, and it is superposed on the pMHD. This component, which we call pELM, exhibits clear similarities with spontaneous ELMs that occur in the same background plasma. It has comparable duration, the magnetic perturbation spectrum extends from low to high frequencies, and the toroidal mode number spectrum exhibits a similar structure and evolution. The lower frequency components have low and positive toroidal mode numbers, while components above 4 kHz evolve from low to high values of $|n|$. Since only a small fraction of the pellet mass is ablated during these time scales, the pELM is likely to be insensitive to the pellet size and mass, but rather dependent on the pedestal parameters, as suggested by the similarities with spontaneous ELMs. The progression from low to high frequency observed in pELMs suggests that a pELM starts as a global, kink-like perturbation, which distorts the plasma and modifies the pressure and current profile locally, causing the excitation of modes with higher values of $n$.

While pELM and pMHD are distinct at high frequencies, the separation is difficult for low frequency modes because of the errors in the measurement of spectra associated with the longer wave periods. While in L-mode and Ohmic phases the amplitude of low frequency component is constant over the total duration of the ablation phase, in H-mode plasmas it has a maximum in a time window centred on the ELM, of duration of about 0.5 ms, much shorter than the ablation phase. Since the toroidal mode number is similar in H-mode and L-mode plasma, it is possible that the initial perturbation induced by the pellet has the same nature, but that the background plasma parameters may have a role in its evolution at later stages. The study of the modified current and pressure profile induced by the pellet, combined with a linear MHD stability analysis are needed in order to understand whether and how the initial pMHD has a role in the triggering of the pELM.

Although the experiments analyzed so far have demonstrated the effectiveness of pellets in triggering ELMs with spectral features similar to spontaneous ELMs, a number of questions still remain unanswered. It is not clear, for example, why pellets injected in H-mode plasmas with isolated type-I or type-III ELM can trigger in some cases isolated pELMs and in other cases compound pELMs. Moreover, having found so far no quantitative differences between the toroidal mode number spectra of spontaneous type-I and type-III ELMs, it is not possible at this stage to conclude how pELMs compare with type-I and type-III spontaneous ELMs.

**Acknowledgments**

The authors acknowledge fruitful discussions with C. Perez and R. Wenninger. This work has been conducted under the European Fusion Development Agreement. The views and opinions expressed herein do not necessarily reflect those of the European Commission. F.M. Poli acknowledges the UK EPSRC for support.

## References

[1] Wagner F *et al*, *Phys. Rev. Lett.* , **49**, 1408 (1982).
[2] Connor J W, *Plasma Phys. Control. Fusion* , **40**, 191 (1998).
[3] Zohm H, *Plasma Phys. Control. Fusion* , **38**, 105 (1996).
[4] Lang P. T, Neuhauser J, Horton L. D *et al*, *Nucl. Fusion*, **43**, 1110 (2003).
[5] Lang P. T, Alper B, Buttery R *et al*, *Nucl. Fusion*, **47**, 754 (2007).
[6] Geraud A, Vinyar I *et al* *The JET high frequency pellet injector*, EFDA-JET-CP(08)04/08, (2008).
[7] Poli FM, Sharapov SE *et al*, *Plasma Phys. Control. Fusion* , **50** 095009 (2008).
[8] Poli FM, Sharapov SE *et al*, *A wavelet-based method to measure the toroidal mode number of ELMs*, proceeding of the ICPP, Fukuoka, accepted for publication in Journal of Plasma and Fusion Research Series.
[9] Figueiredo ACA, Nave MFF, and EFDA-JET Contributors. *Rev. Sci. Instrum.*, **75** 4268, (2004).
[10] De la Luna E, *et al*, *Rev. Sci. Instrum.*, **75**, 3831 (2004).
[11] Heeter R F, Fasoli A F, Ali-Arshad S and Moret J M, *Rev. Sci, Instrum.*, **71**, 4092 (2000).
[12] Sartori R, Saibene G, *et al*, *Plasma Phys. Control. Fusion* , **46**, 723 (2004).
[13] Szepesi T, Kálvn, S, Kocsis G, Lackner K, Lang PT, Maraschek M, Pokol G, P'or and ASDEX Upgrade Team, *Investigation of pellet-driven magnetic perturbations in different tokamak scenarios, submitted to Plasma Phys. Control. Fusion* (2009)
[14] Smeulders P, Conway G D, Alper *et al*, *Plasma Phys. Control. Fusion* , **41**, 1303 (1992).
[15] Perez C. P, Koslowski H. R, Hender T.C. *et al*, *Plasma Phys. Control. Fusion* , **46**, 61 (2004).
[16] Mallat S, *A wavelet tour of signal processing*, chapter 4. Academic Press, Cambridge, (2001).
[17] G. Paschmann and P.W. Daly (Eds.), *Analysis methods for multi-spacecraft data*, chapter 1. International Space Science Institute, Bern, Switzerland (1998).
[18] C. Torrence and G.P. Compo, *Bulletin of the American Meteorological Society*, **79**, 61 (1998).
[19] Beall JM, Kim C and Powers EJ, J. Appl. Phys. **53**, 3933 (1982).
[20] T. Dudok de Wit, V V Krasnosel'skikh, *et al*, Geoph. Res. Lett. **22**, 2653, (1995).
[21] Lang P. T, Alper B, Baylor LR *et al*, *Nucl. Fusion*, **42**, 388 (2002).
[22] Perez C. P, Koslowski H. R, Huysmans G. T. A, *et al*, *Nucl. Fusion*, **44**, 609 (2004).